Stable water isotope behavior during the last glacial maximum: A general circulation model analysis

Jean Jouzel, Randal Koster, Robert Suozzo, Gary Russell

JOURNAL OF GEOPHYSICAL RESEARCH, VOL. 99, NO. D12, PAGES 25,791–25,801, DECEMBER 20, 1994

Stable water isotope behavior during the last glacial maximum: A general circulation model analysis

Jean Jouzel,[1,2] Randal D. Koster,[3] Robert J. Suozzo,[4] and Gary L. Russell[4]

Abstract. Global water isotope geochemistry during the last glacial maximum (LGM) is simulated with an 8° × 10° atmospheric general circulation model (GCM). The simulation results suggest that the "spatial" $\delta^{18}O$/temperature relationships observed for the present-day and LGM climates are very similar. Furthermore, the temporal $\delta^{18}O$/temperature relationship is similar to the present-day spatial relationship in regions for which the LGM/present-day temperature change is significant. This helps justify the standard practice of applying the latter to the interpretation of paleodata, despite the possible influence of other factors, such as changes in the evaporative sources of precipitation or in the seasonality of precipitation. The model suggests, for example, that temperature shifts inferred from ice core data may differ from the true shifts by only about 30%.

1. Introduction

1.1. Isotope/Climate Relationships

The saturation vapor pressure and molecular diffusivity in air of HDO and $H_2{}^{18}O$, the two stable isotopic forms of water, differ from those of $H_2{}^{16}O$, the main component of water. (D represents deuterium, an isotope of hydrogen.) As a result, isotopic fractionation at each phase change of water leads to global-scale variations in the isotope content of precipitation. These variations are well documented [*International Atomic Energy Agency (IAEA)*, 1981; *Craig*, 1961; *Dansgaard*, 1964]: (1) at middle and high latitudes, both δD and $\delta^{18}O$ vary linearly with surface temperature; (2) this relationship does not hold in tropical regions, where isotope concentrations are more significantly influenced by precipitation amount; and (3) δD and $\delta^{18}O$ are linearly related to each other throughout the world with a slope of about 8 and a deuterium excess ($d = \delta D - 8\delta^{18}O$) of about 10‰.

For annual temperatures T below 15°C, the global empirical $\delta^{18}O/T$ relationship can be described by the equation $\delta^{18}O = 0.64T - 12.8$ (see section 3.6.1). We refer to this as the "present-day spatial $\delta^{18}O/T$ relationship" because it is based on observations at spatially distinct measurement sites during the present-day climate. It is conceptually different from the "temporal $\delta^{18}O/T$ relationship," i.e., the relationship describing the variation of $\delta^{18}O$ with T when one stands at a single geographical location and goes back in time through several different climates. Although the temporal $\delta^{18}O/T$ relationship has been studied on decadal timescales [*Rozanski et al.*, 1992], the relationship over climatic timescales is of much greater importance, since it allows the inference of paleotemperatures from measured isotope concentrations in ancient precipitation, for example, as stored in ice sheets, groundwater, and speleothems.

A significant amount of isotope paleodata has already been collected. Continuous sequences are preserved in the snow layers deposited over the ice caps. Detailed isotopic profiles are available in ice cores from Greenland, the Canadian Arctic, and Antarctica, with the longest series extending back about 200,000 years for both Greenland [*Dansgaard et al.*, 1993; *Greenland Ice Core Project (GRIP) Members*, 1993] and Antarctica [*Jouzel et al.*, 1993]. In middle and low latitudes, isotope signatures are measured directly in groundwaters and fluid inclusions in speleothems or tropical ice caps and indirectly in precipitated calcite, tree ring cellulose, and other organic materials, particularly those in lake sediments.

To make use of these data, the paleoclimatologist is often forced to assume that the temporal and present-day spatial $\delta^{18}O/T$ relationships are identical. We now examine this critical assumption through general circulation model (GCM) isotope modeling.

1.2. Isotope Modeling With GCMs

Dynamically simple Rayleigh-type distillation models have been used, with some success, to study observed isotope/climate relationships and thus to evaluate their applicability for paleoclimate study [*Dansgaard*, 1964; *Jouzel and Merlivat*, 1984; *Johnsen et al.*, 1989]. These models, however, cannot adequately account for the complexity of dynamical and microphysical processes leading to the formation of individual precipitation events or for the changes in ocean surface characteristics, in surface topography, and in atmospheric circulation associated with important climatic changes, such as the transition from the last glacial maximum (LGM, around 18,000 years B.P.) to the Holocene. Simply stated, a Rayleigh model that can reproduce the observed present-day behavior of isotopes may still be inadequate in the context of a very different climate.

Many of these shortcomings are avoided by incorporating water isotope cycles into an atmospheric GCM. The GCM approach is straightforward. The ocean, atmosphere, and

[1]Laboratoire de Modélisation du Climat et de l'Environnement, Commisariat à l'Energie Atomique/DSM, Gif-sur-Yvette, France.
[2]Also at Laboratoire de Glaciologie et Géophysique de l'Environnement, CNRS, St. Martin d'Hères, France.
[3]Hydrological Sciences Branch, NASA Goddard Space Flight Center, Greenbelt, Maryland.
[4]NASA Goddard Institute for Space Studies, New York.

Paper number 94JD01819.
0148-0227/94/94JD-01819$05.00

ground reservoirs in the GCM are initialized with reasonable HDO and $H_2{}^{18}O$ concentrations in water, and during a model simulation, the GCM transports the isotope masses through the atmosphere and ground via the same processes used to transport model water (advection, moist convection, reevaporation of falling raindrops, evapotranspiration, etc.). Isotopic fractionation, including kinetic fractionation effects in subsaturated and supersaturated environments, is accounted for at every change of phase. The isotopic tracers do not affect the atmospheric circulation itself.

Joussaume et al. [1984] and *Joussaume* [1983] pioneered this approach, producing global isotope fields for present-day January climate with the GCM of the Laboratoire de Météorologie Dynamique (LMD). *Jouzel et al.* [1987] generated a full annual cycle of isotope fields with the 8° × 10° NASA Goddard Institute for Space Studies (GISS) GCM. Like the LMD model, the GISS model successfully reproduces the important features of present-day global isotope distributions, including the spatial correlations between isotope concentration and temperature at middle to high latitudes and between isotope concentration and precipitation at low latitudes. The robustness of the GISS isotope model has been examined through an extensive sensitivity study [*Jouzel et al.*, 1991]. Isotopic tracers have recently been incorporated [*Hoffmann and Heimann*, 1993] into the ECHAM GCM, the Hamburg version of the European Centre for Medium-Range Weather Forecasts GCM.

A common objective of the GCM isotope modeling efforts is a reconstruction of paleoclimatic isotopic fields to help in the interpretation of paleodata. The studies focus on the LGM because (1) the glacial climate is very different from the current climate, (2) the LGM boundary conditions are sufficiently well known through Climate: Long-Range Investigation, Mapping, and Prediction (CLIMAP) data [*CLIMAP Project Members*, 1981], and (3) isotope paleodata are available for this period in both polar and temperate regions, allowing partial validation of model results. LGM isotope distributions for February and August climates have been obtained with the LMD model [*Joussaume and Jouzel*, 1993]. Presented here are the corresponding GISS model results, which cover the full annual cycle.

2. Simulated LGM Climate

The setup of the LGM simulation paralleled that of the 3-year, present-day simulation of *Jouzel et al.* [1987], differing only in the imposed set of boundary conditions. For example, we assigned a $\delta^{18}O$ increase of 1.6‰ [*Duplessy*, 1981] and an estimated δD increase of 13.5‰ to LGM ocean waters to reflect the volumetric increase of isotopically impoverished ice in polar regions. (Recent work [*Labeyrie et al.*, 1987; *Shackleton*, 1987] leads to a lower estimate of the isotope concentration shift, of about 1.1‰ for $\delta^{18}O$. This can easily be taken into account when interpreting the model results.) Also, sea surface temperatures, sea ice limits, land ice configuration, and land albedo were changed for the LGM simulation according to CLIMAP data [*CLIMAP Project Members*, 1981] with daily values interpolated from climatological monthly means. The CO_2 concentrations in the atmosphere were reduced to 200 ppm (from 315 ppm) in accordance with ice core measurements [*Delmas et al.*, 1980; *Neftel et al.*, 1982]. Orbital parameters such as obliquity and eccentricity were set to their LGM values [*Berger*, 1978].

The formulation of polar snow albedo was modified slightly for the present-day and LGM simulations. The standard GISS GCM parameterization [*Hansen et al.*, 1983] allows the albedo to decrease with snow age. In the simulations discussed here, the albedo of polar snow remained constant at 0.85, resulting in more accurate polar temperatures [*Jouzel et al.*, 1987].

The LGM simulation started on November 1 and ran for 62 months. In addition, the 38-month present-day simulation [*Jouzel et al.*, 1987] was extended an additional 2 years. The first 14 months of both the LGM and present-day simulations were not included in the data analysis to account for model "spin-up"; the isotope diagnostics for both the LGM and present-day simulations thus represent 4-year averages.

Figure 1a displays the simulated field of annual LGM temperatures, and Figure 1b shows the differences between these temperatures and those simulated for the present-day climate [*Jouzel et al.*, 1987]. The largest temperature differences (up to −30°C) are concentrated over the regions corresponding to the LGM's Laurentide and Fennoscandian ice sheets and result largely from the associated elevation changes. A few regions in and around Antarctica show significant temperature reductions during the LGM, but large reductions do not span the continent. The temperature changes simulated in the tropics are generally small. The globally averaged temperature change (LGM minus present) is −4.0°C, which is comparable to the changes obtained in other GCM ice age studies [*Joussaume and Jouzel*, 1993]. The temperature reductions were roughly the same in each season.

On a global basis, precipitation was reduced by 4.4% in the LGM, with systematic reductions over the ice sheet regions. Precipitation increased slightly over some continental areas. A more thorough discussion of the GISS GCM's simulation of LGM climate is provided by *Hansen et al.* [1984] and *Rind and Peteet* [1985].

3. Isotope Behavior During the LGM

The LGM simulation produced the annual $\delta^{18}O$ field shown in Figure 1c. In qualitative agreement with the present-day simulated and observed fields, it is characterized by strong latitudinal gradients near the poles and a breakdown of these gradients in the tropics. The difference map (LGM minus present day) in Figure 1d shows strong reductions in $\delta^{18}O$ over the Fennoscandian and Laurentide ice sheets that are highly correlated with the temperature reductions in Figure 1b, as well as small but positive changes in tropical and subtropical $\delta^{18}O$ that probably reflect the increase in seawater isotope concentration.

The difference map for δD (Figure 1e) shows an equivalent structure. The formulations used for the fractionation and transport of the two isotopes are in fact equivalent, differing only in certain physical parameter values, and thus the model-generated fields of $\delta^{18}O$ and δD provide redundant information about isotope behavior. Figure 1e will prove useful in our comparisons in sections 3.2–3.5 of model results with available paleodata; the discussion of the isotope and temperature relationship in section 3.6, however, will focus on $\delta^{18}O$ alone.

We note in passing that deuterium excess, a measure of the differential behavior of HDO and $H_2{}^{18}O$, may provide important information about a climate's hydrological cycle.

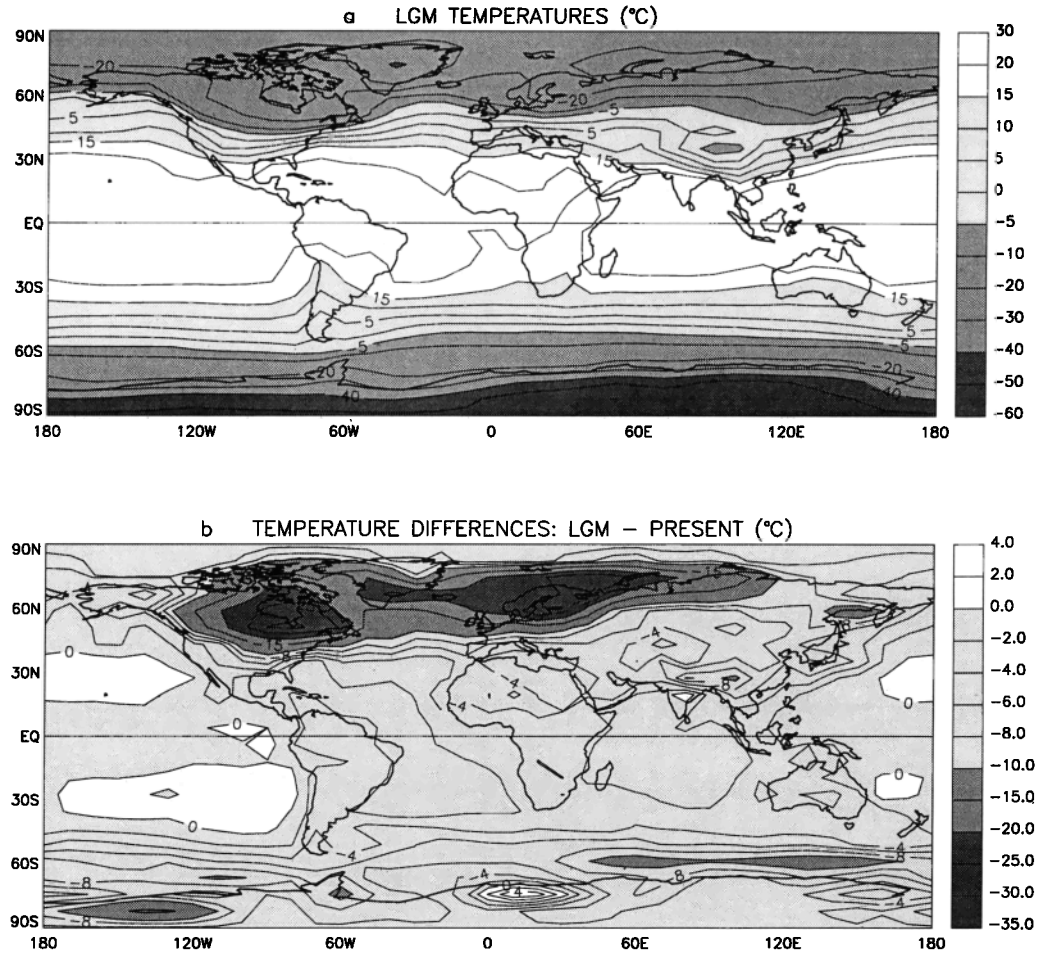

Figure 1. (a) Simulated annual temperatures for the last glacial maximum (LGM) climate (degrees Celsius). (b) Simulated differences in annual temperature, LGM minus present day (degrees Celsius). (c) Simulated annual $\delta^{18}O$ for the LGM climate (per mil). (d) Simulated differences in annual $\delta^{18}O$, LGM to present day (per mil). (e) Simulated differences in annual δD, LGM minus present day (per mil).

For example, numerous studies have tried to relate deuterium excess in polar snow to conditions prevailing in the evaporative source regions of the precipitation, both for present-day [*Johnsen et al.*, 1989; *Petit et al.*, 1991] and past [*Jouzel et al.*, 1982; *Dansgaard et al.*, 1989] climates. A GCM isotope model has potential for more comprehensive studies of deuterium excess [*Joussaume and Jouzel*, 1993; *Jouzel et al.*, 1987].

3.1. Seasonal Cycles

Through a detailed comparison of observations and model results, *Jouzel et al.* [1987] showed that the observed present-day seasonal cycles of $\delta^{18}O$ are generally well simulated by the GCM. One important deficiency, however, of the present-day simulation is the lack of a pronounced $\delta^{18}O$ cycle over Greenland. *Jouzel et al.* [1987] attributed this deficiency to an excessive maritime influence on Greenland precipitation.

During the LGM, increased sea ice extent should reduce this maritime influence and thereby allow a seasonal cycle of $\delta^{18}O$ to develop over Greenland. Figure 2, which compares the simulated seasonal cycles of $\delta^{18}O$ and temperature for the LGM and present-day simulations over several regions, shows that this is indeed the case. The LGM $\delta^{18}O$ cycle over Greenland has an amplitude of about 17‰ and is in phase with the seasonal cycle of temperature.

Over the other ice sheets, the simulated present-day and LGM $\delta^{18}O$ cycles have roughly the same amplitude, with the LGM values shifted down by about the same amount during summer and winter. The amplitude of the $\delta^{18}O$ cycle over central Europe (just south of the ice sheet) is slightly larger during the LGM, probably due to the corresponding increase in the temperature cycle. Other regions show smaller changes. In the equatorial ocean, LGM $\delta^{18}O$ values are similar to (and, as was noted above, slightly higher than) the present-day values through most of the year. The asymmetry noted by *Jouzel et al.* [1987] between seasonal $\delta^{18}O$ behavior in the northern and southern hemispheres is also apparent in the LGM simulation results. In South America (20°S, 50°W), for example, the LGM seasonal cycles of $\delta^{18}O$ and temperature are 6 months out of phase, largely due to the dominance of precipitation amount over temperature in defining isotope distributions in tropical regions.

3.2. The Northern Ice Sheets

Glacial periods are characterized by the buildup of large ice sheets over North America (the Laurentide ice sheet), Greenland, and Scandinavia (the Fennoscandian ice sheet).

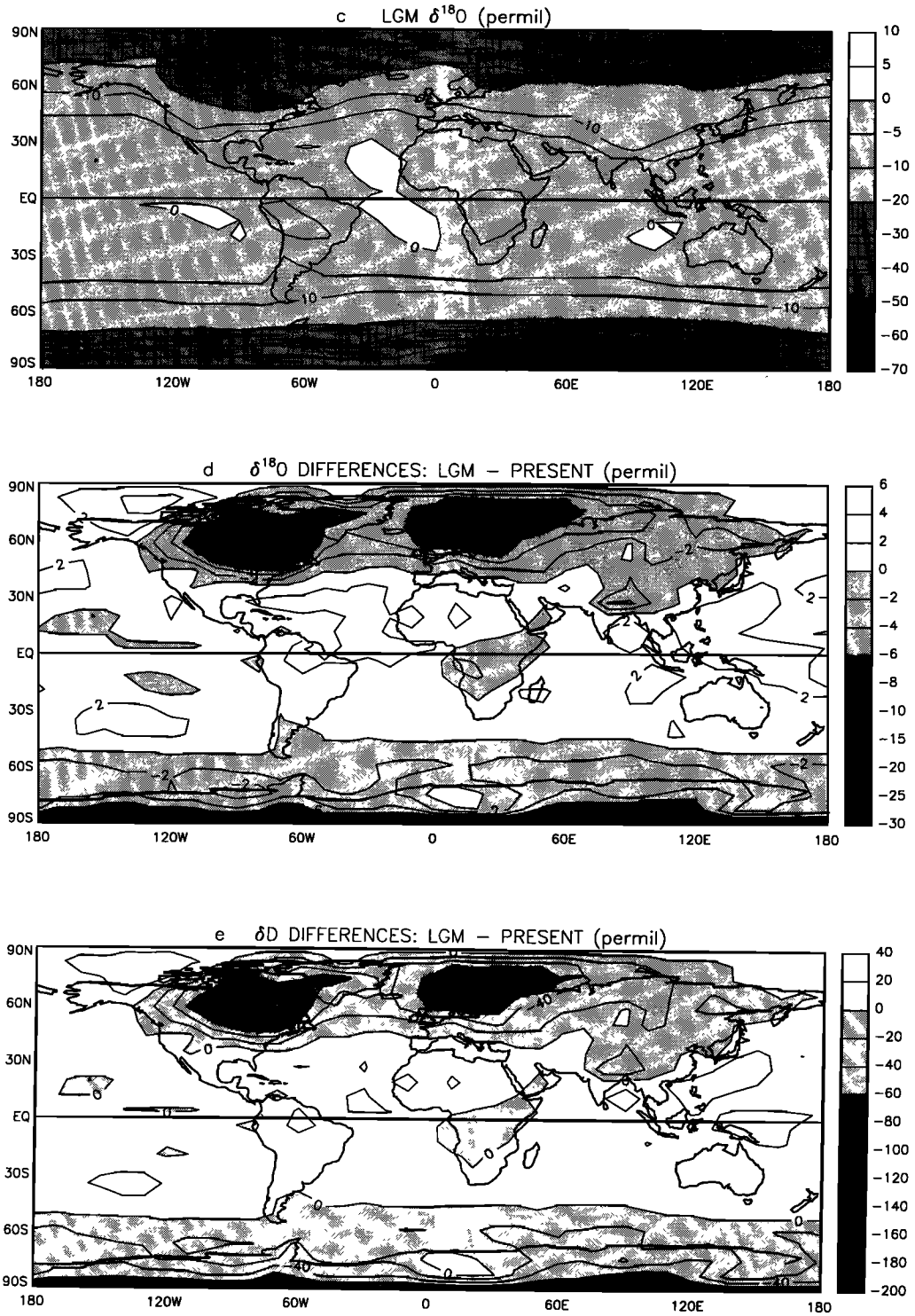

Figure 1. (continued)

Only the Greenland ice sheet still exists, though, and it provides isotope paleodata [*Johnsen et al.*, 1992] for model validation at only three ice core sites. The simulated LGM minus present-day $\delta^{18}O$ shifts at these sites are generally realistic; −7.7‰ versus −6.6‰ observed at the Summit site, −5.8‰ versus −5.0‰ observed at the Renland site, and −6.2‰ versus −12.9‰ observed at Camp Century. Note that a perfect match with the observations is not expected; simulated $\delta^{18}O$ values represent grid square areal averages, whereas observations provide point values. Also, part of the disagreement at Camp Century may reflect the changing altitude of the deposition area [*Johnsen et al.*, 1992; *Raynaud and Lorius*, 1973], which is not included in the model. The observed shift at a fourth Greenland site (Dye 3) is difficult to use because the relevant GCM grid square contains a high ocean fraction.

The minimum $\delta^{18}O$ of precipitation over the Laurentide ice sheet is −37‰, and that over the Fennoscandian ice

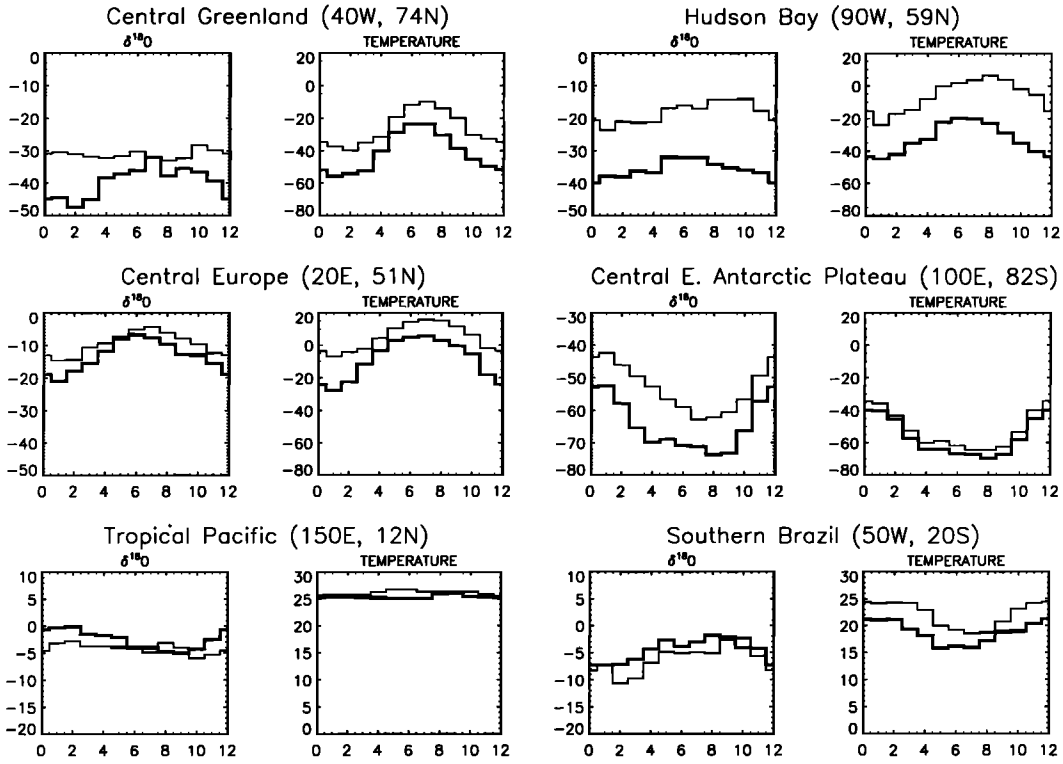

Figure 2. Seasonal cycles of $\delta^{18}O$ (in per mil) and temperature (in degrees Celsius) for six grid squares in different climatic regimes. The light solid lines represent present-day simulation data, and the heavy solid lines represent LGM simulation data.

sheet is −29‰. Since we are simulating the height of the last glacial maximum, the volume-averaged $\delta^{18}O$ within these ice sheets, which is linked to the LGM/present-day $\delta^{18}O$ shift in the ocean, can be no lower than these values. We have some confidence in our simulated minima, since present-day $\delta^{18}O$ distributions are correctly simulated over Antarctica [*Jouzel et al.*, 1987] which has an ice sheet of comparable size. A more quantitative estimate of the volume-averaged $\delta^{18}O$ in these ice sheets can perhaps be obtained with an ice growth model run in conjunction with a GCM isotope model.

3.3. Midlatitudes

Our current understanding of ice age isotope behavior in midlatitudes is based largely on δD and $\delta^{18}O$ measurements in ancient groundwater. Spatial coverage of the groundwater measurement sites is limited; most of the sites lie in Europe and North America, and only a few reside in Asia and in southern hemisphere midlatitudes. Additional data for midlatitude regions have been obtained from tree ring cellulose [*Yapp and Epstein*, 1977], fluid inclusion in speleothems [*Harmon and Schwarcz*, 1981], and precipitated calcite [*Winograd et al.*, 1988, 1992].

Paleowaters from England to Romania indicate that HDO concentrations in European precipitation were lower during the LGM than they are today, by about 12‰ on average and by up to 30‰ in more continental areas [*Rozanski et al.*, 1982; *Ferronski et al.*, 1983]. These paleowaters, however, consist of a mixture of late Pleistocene groundwaters and are difficult to date precisely. Given this uncertainty, we consider our simulated LGM/present-day δD shifts in this part of Europe, which range from about −15‰ to −40‰ with a similar spatial trend (Figure 1e), to be in satisfactory agreement with the observations.

Model validation in North America is more difficult because some of the available observations there are in direct conflict [*Joussaume and Jouzel*, 1993]. Wood cellulose data [*Yapp and Epstein*, 1977], for example, imply that the deuterium content of LGM precipitation over ice-free regions of North America was higher than that of modern precipitation by an average of 19‰, whereas fluid inclusions in speleothems [*Harmon and Schwarcz*, 1981] and groundwater [*Phillips et al.*, 1986] in various parts of the United States suggest consistently negative LGM/present-day δD shifts, from about −10‰ to −25‰. The model predicts a negative shift north of about 40°N and a positive shift south of 40°N in North America. Given the conflict in the observations and the model's inability to resolve details in the strong latitudinal gradients, we deem the comparison between North American observations and simulation results to be inconclusive.

A single LGM/present-day $\delta^{18}O$ shift of about −2‰ has been measured on the Tibetan Plateau [*Thompson et al.*, 1989, 1990] and the simulated shift in the corresponding grid square is about −0.6‰, which is smaller but still negative. Available paleodata in southern hemisphere midlatitudes are essentially limited to measurements in Australia [*Airey et al.*, 1979] and South Africa [*Heaton et al.*, 1986]. The measurements show little or no difference in isotope concentration between modern and glacial waters, in good agreement with the model results.

3.4. Tropics and Subtropics

North African groundwater measurements [*Sonntag et al.*, 1979; *Fontes*, 1980, 1981] provide the only well-documented LGM isotope data available in the tropics and subtropics. The isotope concentrations in these ancient groundwaters are definitely lower than those in present-day precipitation, possibly due [*Rozanski*, 1985] to the occurrence of humid phases in North Africa during glacial times. These humid phases were probably similar to those occurring today in midlatitudes. In fact, North African groundwaters show a west to east δD gradient ($-20‰$ to $-80‰$ from the Atlantic to Egypt) that is comparable to that currently observed over western Europe [*Sonntag et al.*, 1979].

In contrast to the observations, the simulated LGM/present-day δD shifts between 30°N and 30°S are positive except over a few areas in Africa and Asia (Figure 1e). The observed spatial δD gradient for the LGM climate is not reproduced; even though a small gradient exists, simulated LGM δD values lie above $-20‰$ all across North Africa. This model failure results from the lack of a relatively humid climate over North Africa in the LGM simulation; simulated precipitation rates in North Africa are actually lower during the LGM. The proper simulation of climate is clearly a prerequisite to a proper simulation of isotope fields.

Rind and Peteet [1985] studied an apparent inconsistency between the CLIMAP sea surface temperature (SST) data set and tropical paleodata. Through simulations with the GISS model, in which SSTs were artificially decreased by 2°C, they examined the possibility that CLIMAP SSTs are overestimated in tropical regions. In light of this hypothesis, we performed a supplemental, 3-year LGM sensitivity simulation that incorporated the proposed SST reductions. Although the GCM climate and isotope behavior did change slightly to reflect the new SSTs, precipitation rates over North Africa did not increase, and the LGM/present-day δD shifts there were still positive.

The $^{18}O/^{16}O$ ratio in atmospheric O_2 depends in part on the $\delta^{18}O$ of precipitation in the terrestrial biosphere [*Bender et al.*, 1985; *Sowers et al.*, 1993], particularly in the tropics, where much of the photosynthetic production of O_2 occurs. The simulated LGM/present-day $\delta^{18}O$ difference in tropical precipitation is close to the corresponding $\delta^{18}O$ shift in the surface ocean (1.6‰). If this is an accurate result, it would help explain why ice core data show a match between the ^{18}O content of atmospheric O_2 and that of seawater [*Sowers et al.*, 1991, 1993; *Jouzel et al.*, 1993]. We realize, however, that the processes governing isotopic O_2 concentrations may be too complex for such a simple interpretation.

3.5. Isotope Behavior in Antarctica

Four ice cores extending through at least the LGM have been extracted from the Antarctic ice sheet. The LGM/present-day $\delta^{18}O$ shift is remarkably consistent for the three East Antarctic cores; $-5.4‰$ at Dome C [*Lorius et al.*, 1979], $-5‰$ at Vostok [*Lorius et al.*, 1985], and $-5‰$ at Dome B [*Vaikmae et al.*, 1994]. The simulated $\delta^{18}O$ shift of $-5.1‰$, computed from $H_2{}^{16}O$ and $H_2{}^{18}O$ fluxes averaged over 12 grid boxes in the neighborhood of these cores, is realistic. The spatial variability among the grid square data, however, is much too high ($\sigma = 2.7‰$), due in part to a high latitudinal gradient near the pole in the GCM. The average simulated shift of $-3.5‰$ for 10 West Antarctic grid squares in the Byrd area is lower than the observed shift [*Johnsen et al.*, 1972] of $-7‰$, and the simulated shifts again show a high spatial variability ($\sigma = 2.0‰$).

The spatial variability in the simulated $\delta^{18}O$ shifts cannot be attributed to variability in the corresponding temperature shifts because the latter are relatively smooth over Antarctica (Figure 1b). The variability is also unrelated to differences in the evaporative sources of precipitation [*Koster et al.*, 1992] and to differences in precipitation seasonality (as indicated by an examination of the model results at the monthly scale). Instead, it probably results from our use of a second-order scheme for transporting water. When this scheme is replaced by an upstream scheme (which is itself inappropriate due to its high diffusivity [*Jouzel et al.*, 1991]) in a sensitivity test, the variability in the present-day $\delta^{18}O$ fields decreased significantly. Our treatment of microphysical processes, such as isotopic fractionation during snow formation, may also be a contributing factor.

3.6. The $\delta^{18}O$/Temperature Relationship

3.6.1. Spatial relationship. The above comparisons with available paleodata suggest that the GCM, with certain exceptions, reproduces LGM isotope concentrations reasonably well. The model performance appears adequate enough for a global analysis of the LGM and present-day $\delta^{18}O$/temperature relationships. Because this analysis is limited to regions with annual temperatures lower than 15°C, the aforementioned GCM deficiencies in North Africa are avoided.

For the present-day climate the correlation between observed annual precipitation site temperature T (for temperatures below 15°C) and $\delta^{18}O$ in precipitation is strong enough to produce the linear relationship indicated in the scatterplot in Figure 3a. (Each point in the plot corresponds to a single measurement site. The data are derived from the IAEA network and supplemental polar stations [*Jouzel et al.*, 1987].) Figure 3b shows the corresponding plot derived from the GCM's present-day grid square results. The simulated slope, intercept, and scatter produced by the model basically agree with the observations. (See also Table 1.)

The simulated spatial $\delta^{18}O/T$ relationship for the LGM is shown in Figure 3c. This figure and the corresponding statistics in Table 1 demonstrate an important result of this study: on a global scale, the spatial $\delta^{18}O/T$ slope changes by less than 10% with the imposed change in GCM climate. Furthermore, the LGM slope is essentially identical to both the simulated present-day slope and the observed present-day slope when the analysis is limited to regions for which temperatures are greater than −30°C (Table 1). Assigning a lower temperature cutoff is sensible, given the model's seemingly unusual behavior at extremely cold temperatures: a comparison of Figures 3a and 3b shows that the model appears to predict reasonable $\delta^{18}O$ values at −30°C and −60°C but overestimates them in the neighborhood of −40°C.

The agreement of the spatial slopes is indeed remarkable because the LGM and present-day climates are quite different, for example, in their atmospheric circulation, in the prevailing conditions over precipitation source regions, and in the altitudes of precipitation formation. An agreement between present-day and LGM spatial slopes was also found in analogous simulations (for perpetual February and August) with the LMD GCM [*Joussaume and Jouzel*, 1993].

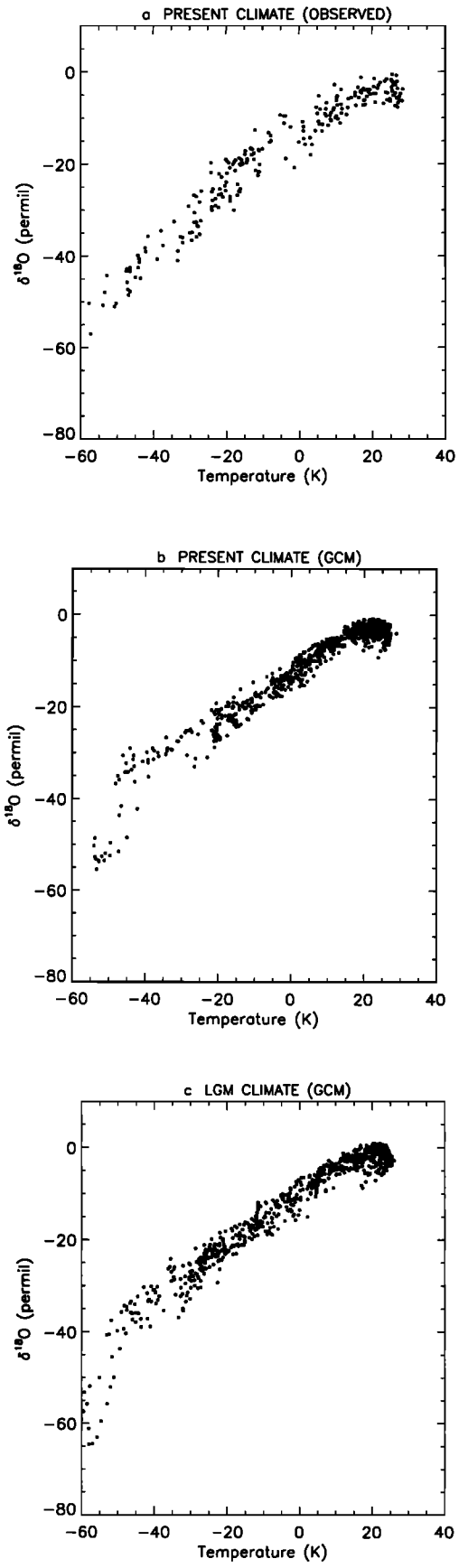

Figure 3. Annual $\delta^{18}O$ in precipitation (in per mil) versus the annual temperature (in degrees Celsius) at the precipitation site, for (a) present-day observations, (b) the present-day GCM simulation, and (c) the LGM GCM simulation.

The LMD GCM's spatial slopes are, in fact, quite comparable to those produced by the GISS model.

Table 1 demonstrates the similarity of the LGM and present-day spatial slopes over individual continental regions. The regional boundaries for most of the regions are as defined by *Jouzel et al.* [1987]. Antarctica is split into western and eastern sections, however, and two additional regions, representing the areas covered by the Laurentide and Fennoscandian ice sheets (where the topographic height increased by more than 250 m), are also examined. The spatial slopes differ the most over Greenland, where the LGM value may be more accurate because of the aforementioned influence of maritime air. The slopes for both climates are clearly highest over Antarctica.

3.6.2. Temporal Relationship. Note that the general agreement between the present-day and LGM spatial slopes does not imply an equivalence between the spatial and temporal $\delta^{18}O/T$ relationships. Unfortunately, the best test of this equivalence would involve a comparison of the spatial slope with the temporal slope obtained for a single region exposed to numerous distinct climates, and the number of climates we can simulate is limited by the availability of suitable boundary conditions.

Here we estimate the temporal slopes with data from the present-day and LGM simulations alone. We compute, at each grid square,

$$\text{slope}_{\text{temporal}} = \frac{\delta^{18}O_{\text{LGM}} - \delta^{18}O_{\text{present}} - 1.6‰}{T_{\text{LGM}} - T_{\text{present}}}. \quad (1)$$

The subtraction of 1.6‰ accounts for the increased seawater isotope concentrations during the LGM. (See section 2). Note that the errors associated with using only two points can be quite large.

Illustrated in Figure 4 is the global distribution of temporal slopes calculated with (1) after applying a simple smoothing algorithm to the simulated temperature and $\delta^{18}O$ fields. The salient feature is the first-order agreement between the temporal slopes and the present-day global spatial slope of 0.6‰/°C. Over most of the globe and in particular over the northern ice sheets, the slope is within 0.2‰/°C of this spatial slope. When the grid square temporal slopes are averaged over specific regions (Table 1), they are found to be similar to (though generally lower than) the corresponding spatial slopes.

Figure 5 shows another method of examining temporal isotope behavior, a scatterplot of $\Delta\delta^{18}O$ against ΔT for the Laurentide ice sheet region. The plot is characterized by a slope of 0.62‰/°C, which is very similar to the simulated spatial slopes. The strong correlation ($r = 0.89$) between $\Delta\delta^{18}O$ and ΔT suggests that about 80% of the temporal changes in isotope concentration on the Laurentide ice sheet can be explained solely by concurrent surface temperature changes despite the LGM/present-day differences in altitude and atmospheric circulation.

In Greenland, the LGM spatial slope may be more accurate than the present-day slope (Table 1) due to the aforementioned influence of maritime air. The slopes might also be affected by changes in the evaporative sources of Greenland precipitation. *Charles et al.* [1994] recently performed a series of independent GCM tracer simulations that show, for present-day and LGM climates, the wide range of evaporative sources contributing to Greenland precipitation. Al-

Table 1. Spatial and Temporal Slopes For Various Regions

Region	Spatial Slopes: Present Day Slope, ‰/°C	Spatial Slopes: Present Day r	Spatial Slopes: LGM Slope, ‰/°C	Spatial Slopes: LGM r	Temporal Slope: Slope, ‰/°C	Temporal Slope: σ, ‰/°C	Average Error of ΔT Prediction, %
			Observations				
Global	0.64	0.96					
Global (−30°C cutoff)	0.57	0.92					
			GCM Results				
Global	0.59	0.96	0.63	0.96	0.50	0.34	−15
Global (−30°C cutoff)	0.57	0.96	0.56	0.97			
Northern hemisphere	0.57	0.97	0.56	0.96	0.36	0.21	−37
Laurentide ice sheet	0.60	0.99	0.66	0.96	0.43	0.15	−28
Fennoscandian ice sheet	0.55	0.99	0.53	0.95	0.45	0.06	−18
Greenland	0.51	0.86	0.77	0.62	0.43	0.04	−15
North America	0.74	0.96	0.55	0.99	0.37	0.10	−50
Eurasia	0.53	0.87	0.45	0.87	0.47	0.12	−13
West Antarctica	0.82	0.94	0.85	0.81	1.09	0.20	32
East Antarctica	1.79	0.84	1.70	0.89	1.30	0.36	−27

The regional boundaries are as defined by *Jouzel et al.* [1987]. Antarctica is split into western and eastern sections, however, and two additional regions, representing the areas covered by the Laurentide and Fennoscandian ice sheets (where the topographical height increased by more than 250 m), are also examined. Grid squares for which annual temperatures exceed 15 degrees Celsius are excluded from the analyses. The temporal slopes (LGM minus present day) are computed from smoothed data.

though each evaporative source has a different isotopic signature and although the relative strengths of the sources do differ between the climates (particularly on the seasonal time scale), the results in Table 1 and Figure 4 suggest that these differences are not sufficient to undermine the current interpretation of Greenland isotopic paleodata [*Dansgaard et al.*, 1989, 1993; *GRIP Members*, 1993] as indicators of paleoclimatic temperature variations. Interpretations of temperature borehole profiles [*Johnsen et al.*, 1992]) provide observational evidence that most of the temporal isotope variation in Greenland is indeed related to variations in site temperature.

The relatively high slopes simulated in Antarctica (Figure 4) deserve comment. The temporal slopes show an unrealistic poleward increase, with values ranging from 0.6‰/°C in coastal regions to about 2‰/°C in central Antarctica. The poleward increase is probably an artifact of the GCM calculations, for two reasons: (1) a gradient in $\delta^{18}O$ shift is not seen in measurements at the Dome C and Vostok sites, and (2) the temporal slopes show a poleward decrease in the LMD model [*Joussaume and Jouzel*, 1993], which uses a different transport scheme. Nevertheless, the GCM does appear to capture some important aspects of isotope behavior in East Antarctica. Observations there suggest a spatial slope of 1.12‰/°C when $\delta^{18}O$ is correlated against the temperature above the inversion layer, which better represents the temperature of precipitation formation [*Robin*, 1977]. This exceeds the corresponding slope over Greenland and other areas and is in excellent agreement with the slope (1.1–1.2‰/°C) derived from a Rayleigh model that includes kinetic fractionation at snow formation [*Jouzel and Merlivat*, 1984]. A similar temporal slope (1.26‰/°C) is derived from the GCM results when $\delta^{18}O$ in East Antarctic precipitation is examined against the temperature in the GCM's second

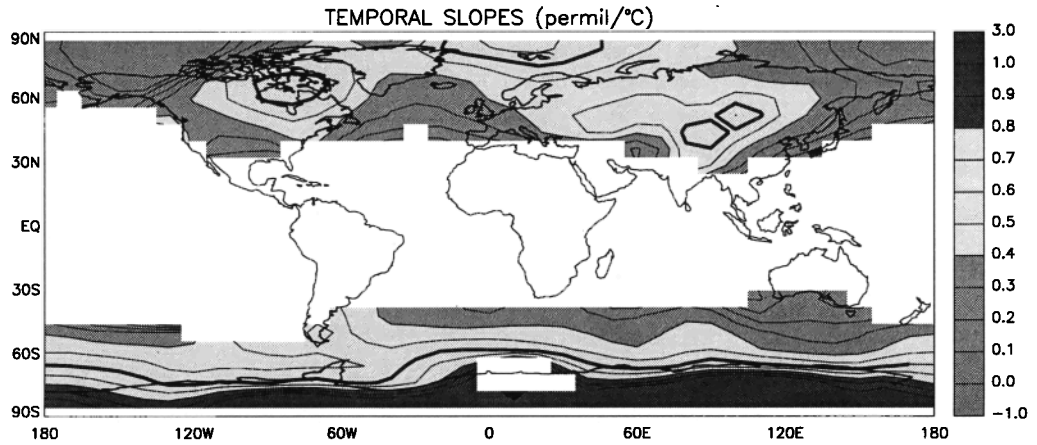

Figure 4. Global distribution of temporal $\delta^{18}O/T$ slopes estimated from GCM simulation results with (1). Slopes are not shown in regions where the LGM/present-day temperature difference is less than 3°, due to background noise, or where the temperature in either climate exceeds 15°C. The 0.6‰/°C contour is shown as a heavy solid line.

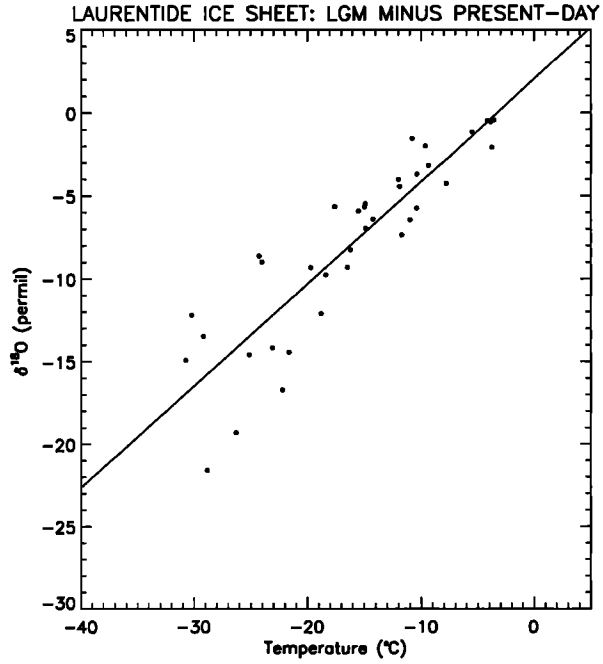

Figure 5. Simulated changes (LGM minus present-day) of $\delta^{18}O$ in precipitation (in per mil) versus the corresponding changes in annual precipitation site temperature (in degrees Celsius), for the Laurentide ice sheet.

lowest atmospheric layer, which lies above the inversion layer.

We conclude the comparison of the spatial and temporal slopes with a quantitative evaluation of the appropriateness of using a present-day spatial slope to estimate temporal temperature shifts. Associated with each region in Table 1 is a present-day spatial slope, and simulated for each grid square in the region is a LGM/present-day $\delta^{18}O$ shift. This is exactly the type of information available, for example, at an ice core site. The spatial slope and $\delta^{18}O$ shift are combined to produce an estimated LGM/present-day temperature shift at each square, which is directly compared to the corresponding actual (simulated) temperature shift. The average relative error for each region is shown in the final column of Table 1. (Smoothed temperature and $\delta^{18}O$ fields are again used for the temporal analysis. The regional averaging hides significant spatial variability in the errors.) Errors are high in some regions, for example, 50% in North America. Over the ice sheets, though, the average relative errors in the estimated temperature shifts are of the order of 30% or less. These error estimates are similar to those obtained with the LMD model [*Joussaume and Jouzel*, 1993].

The GCM results suggest that spatial slopes seem on average to be adequate surrogates for temporal slopes. More fundamentally, they support the interpretation of isotopic ice core data in terms of local temperature changes, at least for large signals less affected by noise.

4. Summary

The success of the GISS GCM isotope model in simulating the present-day global geochemistry of water isotopes has been established elsewhere [*Jouzel et al.*, 1987]. Here we use the model to simulate isotope geochemistry during the LGM. Only limited amounts of paleodata are available for validation of the simulation results. The GCM reproduces LGM isotope behavior reasonably well over Greenland and in most midlatitude regions, though the comparisons over North America are inconclusive. Simulated LGM δD values over North Africa are unrealistic. The LGM/present-day $\delta^{18}O$ shifts simulated in Antarctica agree on average with the measured shifts but show excessive spatial variability.

This study addresses a fundamental question in paleoclimatology: Does the observed present-day spatial $\delta^{18}O/T$ relationship also hold in time, that is, at a single location exposed to numerous distinct climates? Only two different climates were used to derive the temporal slope distribution seen in Figure 4, so the distribution is highly approximate. Nevertheless, the GCM results suggest that over wide areas, the spatial and temporal slopes roughly agree. (A related result is that the LGM and present-day $\delta^{18}O/T$ spatial relationships are very similar). Although certain aspects of the results over Antarctica are not satisfying, the simulated global fields of $\delta^{18}O$, and in particular those values obtained over the Laurentide ice sheet, support the current use of the observed present-day spatial slope for interpreting ice core data in terms of local temperature changes, with an average relative error of the order of 30% or less.

Acknowledgments. Wallace Broecker, James White, Reto Ruedy, and David Rind were very helpful during all phases of this research. Alexandre Armengaud helped with the model runs. The Goddard Institute for Space Studies (and thus the NASA Climate Program) provided computational and financial support. Financial support also came from the French Programme National d'Etudes de la Dynamique du Climat.

References

Airey, P. L., G. E. Calf, B. L. Campbell, P. E. Hartley, D. Roman, and M. A. Habermehl, Aspects of the isotope hydrology of the Great Artesian Basin, Australia, in *Isotope Hydrology 1978*, pp. 205–219, International Atomic Energy Agency, Vienna, 1979.

Bender, M. L., L. D. Labeyrie, D. Raynaud, and C. Lorius, Isotopic composition of atmospheric O_2 in ice linked with deglaciation and global primary productivity, *Nature*, *318*, 349–352, 1985.

Berger, A. L., Long-term variations of daily insolation and Quaternary climatic changes, *J. Atmos. Sci.*, *35*, 2362–2367, 1978.

Charles, C. D., D. Rind, J. Jouzel, R. D. Koster, and R. G. Fairbanks, Glacial-interglacial changes in moisture sources for Greenland: Influences on the ice core record of climate, *Science*, *263*, 508–511, 1994.

Climate: Long-Range Investigation, Mapping, and Prediction (CLIMAP) Project Members, Seasonal reconstruction of the Earth's surface at the last glacial maximum, *Map Chart Ser.*, *36*, Geol. Soc. of Am., Boulder, Colo., 1981.

Craig, H., Isotopic variation in meteoric waters, *Science*, *133*, 1702–1703, 1961.

Dansgaard, W., Stable isotopes in precipitation, *Tellus*, *16*, 436–468, 1964.

Dansgaard, W., J. W. C. White, and S. J. Johnsen, The abrupt termination of the Younger Dryas climate event, *Nature*, *339*, 532–534, 1989.

Dansgaard, W., et al., Evidence for general instability of past climate from a 250-kyr ice-core record, *Nature*, *364*, 218–220, 1993.

Delmas, R., J. M. Ascensio, and M. Legrand, Polar ice evidence that atmospheric CO_2 20,000 y BP was 50% of present, *Nature*, *284*, 155–157, 1980.

Duplessy, J. C., Oxygen isotope studies and Quaternary marine climates, in *Climatic Variations and Variability: Facts and Theories*, edited by A. Berger, pp. 181–192, D. Reidel, Norwell, Mass., 1981.

Ferronski, V. I., L. S. Vlasova, A. D. Esikov, V. A. Polakov, Y. B. Seletski, M. J. Punning, and R. A. Vaikmae, Relationships between climatic changes and variations in isotopic composition of groundwater precipitation and organic soil matter in the Quaternary period, in *A Collection of Environmental Isotope Studies*, pp. 13–35, International Atomic Energy Agency, Vienna, 1983.

Fontes, J. C., Environmental isotopes in groundwater hydrology, in *Handbook of Environmental Geochemistry*, vol. 1, *The Terrestrial Environment*, pp. 75–140, edited by P. Fritz and J. C. Fontes, Elsevier, New York, 1980.

Fontes, J. C., Paleowaters, in *Stable Isotope Hydrology, Deuterium and ^{18}O in the Water Cycle*, pp. 273–298, International Atomic Energy Agency, Vienna, 1981.

Greenland Ice Core Project (GRIP) Members, Climate instability during the last interglacial period recorded in the GRIP ice core, *Nature*, *364*, 203–207, 1993.

Hansen, J., G. Russell, D. Rind, P. Stone, A. Lacis, S. Lebedeff, R. Ruedy, and L. Travis, Efficient three-dimensional global models for climate studies: Models I and II, *Mon. Weather Rev.*, *111*, 609–662, 1983.

Hansen, J., A. Lacis, D. Rind, G. Russell, P. Stone, I. Fung, R. Ruedy, and J. Lerner, Climate sensitivity: Analysis of feedback mechanisms, in *Climate Processes and Climate Sensitivity*, *Geophys. Monogr. Ser.*, vol. 29, edited by J. E. Hansen and T. Takahashi, pp. 130–163, AGU, Washington, D. C., 1984.

Harmon, R. S., and H. P. Schwarcz, Changes of ^{2}H and ^{18}O enrichment of meteoric water and Pleistocene glaciation, *Nature*, *290*, 125–128, 1981.

Heaton, T. H. E., A. S. Talma, and J. C. Vogel, Dissolved gas paleotemperatures and ^{18}O variations derived from groundwater near Uitenhage, South Africa, *Quat. Res.*, *25*, 79–88, 1986.

Hoffmann, G., and M. Heimann, Water tracers in the ECHAM general circulation model, in Isotope Techniques in the Study of Past and Current Environmental Changes: Proceedings of an International Symposium, *IAEA-SM-329/7*, pp. 3–14, Vienna, 1993.

International Atomic Energy Agency (IAEA), Statistical treatment of environmental isotope data in precipitation, *Tech. Rep. Ser.* Rep./Int. At. Energy Agency, *206*, pp. 1–256, Vienna, 1981.

Johnsen, S. J., W. Dansgaard, H. B. Clausen, and C. C. Langway Jr., Oxygen isotope profiles through the Antarctic and Greenland ice sheets, *Nature*, *235*, 429–434, 1972.

Johnsen, S. J., W. Dansgaard, and J. W. C. White, The origin of Arctic precipitation under present and glacial conditions, *Tellus*, *Ser. B*, *41*, 452–468, 1989.

Johnsen, S. J., H. B. Clausen, W. Dansgaard, K. Fuhrer, N. Gundestrup, C. U. Hammer, P. Iversen, J. Jouzel, B. Stauffer, and J. P. Steffensen, Irregular glacial interstadials recorded in a new Greenland ice core, *Nature*, *359*, 311–313, 1992.

Joussaume, S., Modélisation des cycles des espèces isotopiques de l'eau et des aérosols d'origine désertique dans un modèle de circulation générale de l'atmosphère, thesis, 226 pp., Univ. of Paris, Paris, 1983.

Joussaume, S., and J. Jouzel, Paleoclimatic tracers: An investigation using an atmospheric general circulation model under ice age conditions, 2, Water isotopes, *J. Geophys. Res.*, *98*, 2807–2830, 1993.

Joussaume, S., R. Sadourny, and J. Jouzel, A general circulation model of water isotope cycles in the atmosphere, *Nature*, *311*, 24–29, 1984.

Jouzel, J., and L. Merlivat, Deuterium and oxygen 18 in precipitation: Modeling of the isotopic effects during snow formation, *J. Geophys. Res.*, *89*, 11,749–11,757, 1984.

Jouzel, J., L. Merlivat, and C. Lorius, Deuterium excess in an East Antarctic ice core suggests higher relative humidity at the oceanic surface during the last glacial maximum, *Nature*, *299*, 688–691, 1982.

Jouzel, J., G. Russell, R. Suozzo, R. Koster, J. White, and W. Broecker, Simulations of the HDO and H_2 ^{18}O atmospheric cycles using the NASA GISS general circulation model: The seasonal cycle for present-day conditions, *J. Geophys. Res.*, *92*, 14,739–14,760, 1987.

Jouzel, J., R. Koster, R. Suozzo, G. Russell, J. White, and W. Broecker, Simulations of the HDO and H_2 ^{18}O atmospheric cycles using the NASA GISS general circulation model: Sensitivity experiments for present-day conditions, *J. Geophys. Res.*, *96*, 7495–7507, 1991.

Jouzel, J., et al., Extending the Vostok ice-core record of paleoclimate to the penultimate glacial period, *Nature*, *364*, 407–412, 1993.

Koster, R., J. Jouzel, R. Suozzo, and G. Russell, Origin of July Antarctic precipitation and its influence on deuterium content: A GCM analysis, *Clim. Dyn.*, *7*, 195–203, 1992.

Labeyrie, L. D., J. C. Duplessy, and P. L. Blanc, Variations in mode of formation and temperature of oceanic deep waters over the past 125,000 years, *Nature*, *327*, 477–482, 1987.

Lorius, C., L. Merlivat, J. Jouzel, and M. Pourchet, A 30,000 yr isotope climatic record from Antarctic ice, *Nature*, *280*, 644–648, 1979.

Lorius, C., J. Jouzel, C. Ritz, L. Merlivat, N. I. Barkov, Y. S. Korotkevich, and V. M. Kotlyakov, A 150,000 year climatic record from Antarctic ice, *Nature*, *316*, 591–596, 1985.

Neftel, A., H. Oeschger, J. Schwander, B. Stauffer, and R. Zumbrunn, Ice core sample measurements give atmospheric CO_2 content during the past 40,000 years, *Nature*, *295*, 220–223, 1982.

Petit, J. R., J. W. C. White, N. W. Young, J. Jouzel, and Y. S. Korotkevich, Deuterium excess in recent Antarctic snow, *J. Geophys. Res.*, *96*, 5113–5122, 1991.

Phillips, F. M., L. A. Peeters, and M. K. Tansey, Paleoclimatic inferences from an isotopic investigation of groundwater in the central San Juan Basin, New Mexico, *Quat. Res.*, *26*, 179–193, 1986.

Raynaud, D., and C. Lorius, Climatic implications of total gas content in ice at Camp Century, *Nature*, *243*, 283–284, 1973.

Rind, D., and D. Peteet, Terrestrial conditions at the last glacial maximum and CLIMAP sea-surface temperature estimates: Are they consistent?, *Quat. Res.*, *24*, 1–22, 1985.

Robin, G. de Q., Ice cores and climatic changes, *Philos. Trans. R. Soc. London B*, *280*, 143–168, 1977.

Rozanski, K., C. Sonntag, and K. O. Munnich, Factors controlling stable isotope composition of European precipitation, *Tellus*, *34*, 142–150, 1982.

Rozanski, K., Deuterium and oxygen-18 in European groundwaters—links to atmospheric circulation in the past, *Chem. Geol.*, *52*, 349–363, 1985.

Rozanski, K., L. Araguas-Araguas, and R. Gonfiantini, Relation between long-term trends of oxygen-18 isotope composition of precipitation and climate, *Science*, *258*, 981–984, 1992.

Shackleton, N. J., Oxygen isotopes, ice volume and sea level, *Quat. Sci. Rev.*, *6*, 183–190, 1987.

Sonntag, C., E. Klitzcsch, E. P. Lohnert, E. M. El-Shazly, K. O. Munnich, C. Junghans, U. Thorweihe, K. Weistroffer, and F. M. Swailem, Paleoclimatic information from deuterium and oxygen-18 in carbon-14 dated north Saharian groundwaters, in *Isotope Hydrology 1978*, vol. II, pp. 569–581, International Atomic Energy Agency, Vienna, 1979.

Sowers, T., M. Bender, D. Raynaud, Y. S. Korotkevich, and J. Orchado, The ^{18}O record of atmospheric O_2 from air inclusions in the Vostok ice core: Timing of CO_2 and ice volume changes during the penultimate deglaciation, *Paleoceanography*, *6*, 679–696, 1991.

Sowers, T., M. Bender, L. Labeyrie, D. Martinson, J. Jouzel, D. Raynaud, J. J. Pichon, and Y. S. Korotkevich, 135,000-year Vostok-SPECMAP common temporal framework, *Paleoceanography*, *8*, 737–766, 1993.

Thompson, L. G., E. Mosley-Thompson, M. E. Davis, J. F. Bolzan, J. Dai, T. Yao, N. Gundestrup, X. Wu, L. Klein, and Z. Xie, Holocene–late Pleistocene climatic ice core records from Qinghai-Tibetan Plateau, *Science*, *246*, 474–477, 1989.

Thompson, L. G., E. Mosley-Thompson, M. E. Davis, J. F. Bolzan, J. Dai, L. Klein, N. Gundestrup, T. Yao, X. Wu, and Z. Xie, Glacial stage ice-core record from the subtropical Dundee ice cap, China, *Ann. Glaciol.*, *14*, 288–297, 1990.

Vaikmae, R., J. Jouzel, J. R. Petit, and M. Stievenard, A new Antarctic climate record from the Dome B ice core, paper presented at Isotopic Techniques in the Study of Past and Current Environmental changes in the Hydrosphere and Atmosphere, April 19–23, 1993, Int. At. Energy Agency, Vienna, 1993.

Winograd, I. J., B. J. Szabo, T. B. Coplen, and A. C. Riggs, A 250,000-year climatic record from Great Basin vein calcite: Implications for Milankovich theory, *Science*, *242*, 1275–1280, 1988.

Winograd, I. J., T. B. Coplen, J. M. Landwehr, A. C. Riggs, K. R. Ludwig, B. J. Szabo, P. T. Kolesar, and K. M. Revetz, Continuous 500,000 year climatic record from vein calcite in Devils Hole, Nevada, *Science*, *258*, 255–260, 1992.

Yapp, C. J., and S. Epstein, Climatic implication of D/H ratios of meteoric water over North America (9500–22,000 BP) as inferred from ancient wood cellulose C-H hydrogen, *Earth Planet. Sci. Lett.*, *34*, 333–350, 1977.

J. Jouzel, Laboratoire de Modélisation du Climat de l'Environnement, CEA/DSM, Bâtiment 709, Orme des Merisiers, CE Saclay 91191 Gif-sur-Yvette Cedex, France. (e-mail: jouzel@asterix.saclay.cea.fr)

R. D. Koster, Hydrological Sciences Branch, NASA Goddard Space Flight Center, MC 974, Greenbelt, MD 20771. (e-mail: randy@worldh2o.gsfc.nasa.gov)

G. L. Russell and R. J. Souzzo, NASA Goddard Institute for Space Studies, 2880 Broadway, New York, NY 10025.

(Received October 14, 1993; revised July 8, 1994; accepted July 11, 1994.)